REPORT DOCUMENTATION PAGE

Form Approved
OMB No. 0704-0188

1. REPORT DATE *(DD-MM-YYYY)*	2. REPORT TYPE	3. DATES COVERED *(From - To)*
2006	Open Literature	

4. TITLE AND SUBTITLE
A Physiologically Based Pharmacokinetic (PB/PK) Model for Multiple Exposure Routes of Soman in Multiple Species

5a. CONTRACT NUMBER
DAA019-02-0-0001 (DO 0573)

5b. GRANT NUMBER

5c. PROGRAM ELEMENT NUMBER

6. AUTHOR(S)
Sweeney, RE, Langenberg, JP, Maxwell, DM

5d. PROJECT NUMBER

5e. TASK NUMBER

5f. WORK UNIT NUMBER

7. PERFORMING ORGANIZATION NAME(S) AND ADDRESS(ES)

US Army Medical Research Institute of Chemical Defense
ATTN: MCMR-CDR
3100 Ricketts Point Road
Aberdeen Proving Ground, MD 21010-5400 and
RESECO, PO Box 554
Nottingham, PA 19262

8. PERFORMING ORGANIZATION REPORT NUMBER

USAMRICD-P06-005

9. SPONSORING / MONITORING AGENCY NAME(S) AND ADDRESS(ES)

US Army Medical Research Institute of Institute of Chemical Defense
ATTN: MCMR-CDZ-P
3100 Ricketts Point Road
Aberdeen Proving Ground, MD 21010-5400

10. SPONSOR/MONITOR'S ACRONYM(S)

11. SPONSOR/MONITOR'S REPORT NUMBER(S)

12. DISTRIBUTION / AVAILABILITY STATEMENT

Approved for public release; distribution unlimited

13. SUPPLEMENTARY NOTES
Published in Archives of Toxicology, 80, 719-731, 2006.

14. ABSTRACT
See reprint.

15. SUBJECT TERMS
Pharmacokinetic model, nerve agent, soman, exposure route, computer simulation

16. SECURITY CLASSIFICATION OF:			17. LIMITATION OF ABSTRACT	18. NUMBER OF PAGES	19a. NAME OF RESPONSIBLE PERSON
a. REPORT	b. ABSTRACT	c. THIS PAGE			Donald Maxwell
UNLIMITED	UNLIMITED	UNLIMITED	UNLIMITED	11	19b. TELEPHONE NUMBER *(include area code)* 410-436-1315

Arch Toxicol (2006) 80: 719–731
DOI 10.1007/s00204-006-0114-0

TOXICOKINETICS AND METABOLISM

Richard E. Sweeney · Jan P. Langenberg
Donald M. Maxwell

A physiologically based pharmacokinetic (PB/PK) model for multiple exposure routes of soman in multiple species

Received: 6 March 2006 / Accepted: 25 April 2006 / Published online: 23 May 2006

Abstract A physiologically based pharmacokinetic (PB/PK) model has been developed in advanced computer simulation language (ACSL) to describe blood and tissue concentration–time profiles of the C(±)P(−) stereoisomers of soman after inhalation, subcutaneous and intravenous exposures at low (0.8–1.0 × LD_{50}), medium (2–3 × LD_{50}) and high (6 × LD_{50}) levels of soman challenge in three species (rat, guinea pig, marmoset). Allometric formulae were used to compute the compartment volumes, blood flow rates, tidal volume and respiratory rate based upon total animal weight. Blood/tissue partition coefficients for soman, initial carboxylesterase and acetylcholinesterase levels and the rate constants for interactions between soman and these enzymes were species-dependent and were obtained from in vitro measurements reported in the literature. The model incorporated arterial and venous blood, lung, kidney, liver, richly perfused, poorly perfused and fat tissue compartments as well as subcutaneous and nasal exposure site compartments. First-order absorption from linearly filled soman deposits into metabolizing exposure site compartments was employed to model subcutaneous and inhalation exposures. The model was validated by comparing the predicted and observed values for C(±)P(−)-soman in arterial blood at various times following exposure and by regression analysis. Sensitivity analysis was used to determine the effects of perturbations in the model parameters on the time-course of arterial C(−)P(−)-soman concentrations for different exposure routes. In our evaluation of 28 datasets, predicted values were generally within 95% confidence limits of the observed values, and regression coefficients comparing predicted and observed data were greater than 0.85 for 95% of the intravenous and subcutaneous datasets and 25% of the inhalation datasets. We conclude that the model predicts the soman toxicokinetics for doses ≥1 × LD_{50} for intravenous and subcutaneous exposures and inhalation exposures of 8 min or less sufficiently well to allow its use in the modeling of bioscavenger protection.

R. E. Sweeney (✉)
RESECO Research Engineering Consultants,
P.O. Box 554, Nottingham, PA 19362, USA
E-mail: Richard.Sweeney@us.army.mil
Tel.: +1-410-4364137
Fax: +1-410-4368377

J. P. Langenberg
TNO Defence, Security and Safety,
P.O. Box 45, 2280 AA Rijswijk, The Netherlands

D. M. Maxwell
US Army Medical Research Institute of Chemical Defense,
3100 Ricketts Point Road, Aberdeen Proving Ground,
Aberdeen, MD 21010-5400, USA

Introduction

Computer simulations based upon mathematical models have long been used to study the effects of a specific perturbation on systems in which it is impossible to measure these effects for either technical or ethical reasons. Studies involving living systems often fall into this category when the extrapolation of animal data to humans is desired. To provide reliable predictions for a particular animal species, a numerical model should account for pertinent physiological and biochemical pathways and should use only parameters that can ethically be measured in that species. If such a model can be validated against observed data in several test species, then there is a high degree of confidence that the model will provide adequate predictions in a new species when parameters for that species are used. Physiologically based pharmacokinetic (PB/PK) models were developed as a method for extrapolating between species (Gerlowski and Jain 1983). Such models make predictions based solely on measurable inputs and known physiological structure. Generally, PB/PK model predictions do not match the observed data points as well as models incorporating parameters that have been estimated by

classical pharmacokinetic curve fitting to single data sets. However, the strength of the PB/PK models lies in the fact that they can be extrapolated to new species with confidence (Gibaldi and Perrier 1982).

We are ultimately interested in predicting the blood and tissue concentrations of nerve agents in humans. Toward that end, we have augmented a previously reported PB/PK model (Langenberg et al. 1997) that described the blood and tissue concentrations of the organophosphorus (OP) nerve agent soman (1,2,2-trimethylpropyl methylphosphonofluoridate) after intravenous exposures at several challenge levels in guinea pigs. Incorporated in the updated model is the ability to extrapolate between species and to model subcutaneous and inhalation exposures in addition to intravenous injections. Allometric formulae (Fiserova-Begerova and Hughes 1983) were used to compute compartment volumes and flows based upon an animal's body weight. This model combines similar tissues into groups to describe richly perfused and poorly perfused compartments. Also, a fat tissue compartment has been introduced to model a nonreactive soman depot. The model was validated against the available published soman blood concentration data (Benschop and De Jong 2001) collected after intravenous, subcutaneous and inhalation exposure in guinea pigs, rats, and marmosets.

Methods

Animal models

The data used for testing this PB/PK model was obtained from the review by Benschop and DeJong (2001) in which the toxicokinetics of soman were measured in male Wistar (WAG/Rij) rats (250 g), Dunkin–Hartley male guinea pigs (500 g), and male marmosets (*Callithrix jacchius*) (357 g).

Model development

Figure 1 presents the interconnections between the compartments used in this model. For each compartment, equations were derived that simulated the chemical interactions between each toxic P(−)-soman stereoisomer with acetylcholinesterase (AChE, EC 3.1.1.7), carboxylesterase (CaE, EC 3.1.1.1), and an OP-hydrolase enzyme (EC 3.1.8.2). Mass transport for soman was modeled using a flow-limited design with well-mixed compartments in which the blood leaving a compartment is in equilibrium with the compartment's tissue. Reaction rate parameters, partition coefficients, and initial enzyme concentrations in the compartments were estimated as reported by Langenberg et al. (1997) from in vitro measurements of tissue samples. The rapidly detoxified C(±)P(+)-soman stereoisomers were not treated in this model.

Intravenous exposures were mathematically treated as mass infusions directly into the venous blood compartment at a constant rate for 6 s (bolus injections) or for 8 min (intravenous infusion). Subcutaneous exposure was modeled as a constant mass infusion into a subcutaneous deposit during a 6-s injection period with a simultaneous first-order release from the deposit into a subcutaneous tissue compartment. Incorporation of a subcutaneous tissue compartment allows the tissue that is directly affected by the injection to be treated separately from the bulk of the skin and muscle tissue, which were lumped into the poorly perfused compartment. The volume of the subcutaneous deposit was set equal to the injectate volume. The volume of the subcutaneous tissue compartment was estimated to be ten times the injectate volume. The flow for the compartment was computed (using a volume percentage) from the poorly perfused compartment flow.

Ainsworth and Shephard (1961), using cross-respiration experiments in rabbits and monkeys, have demonstrated that inhaled nerve agent enters the body through the upper airway and nasal tissues and not through the lungs. Accordingly, inhalation dosing was treated as a constant rate of soman deposition into a nasal deposit (representing the mucosal layer) followed by first-order absorption from that deposit into a nasal tissue compartment (see Fig. 1). The nasal tissue compartment is intended to incorporate those portions of the nasal and upper respiratory tissue that are first affected by the soman. Detoxifying reactions with soman were assumed to occur in this nasal tissue compartment, which was estimated to be 1% of the total body weight.

The compartment volume and blood flows were computed within the model using formulae developed to describe physiological parameters in many species from body weight (Fiserova-Begerova and Hughes 1983). In cases where more than a single formula was available for estimating a particular parameter, the model averaged the available estimates. The chemical interactions modeled in each compartment included irreversible binding of the C(±)P(−)-soman stereoisomers with AChE and CaE, which were described using bimolecular reaction rate constants. A first-order elimination of soman was used to model excretion and hydrolysis (both chemical and enzymatic) in the blood, kidney and liver compartments.

In each model compartment, mass-balance equations were used to derive a set of coupled first-order differential equations describing the soman and enzyme concentrations. The resulting differential equations were programmed in advanced computer simulation language (ACSL) and solved numerically using the acslXtreme package (AEgis Technologies Group, Inc., Huntsville, AL) running on a desktop computer (Windows XP, 128 MB RAM). The arterial compartment C(±)P(−)-soman concentrations from the model simulations were exported into data files and plotted along with observed data points reported by Benschop and De Jong (2001) using Prism3 (GraphPad Software Incorporated, San Diego, CA).

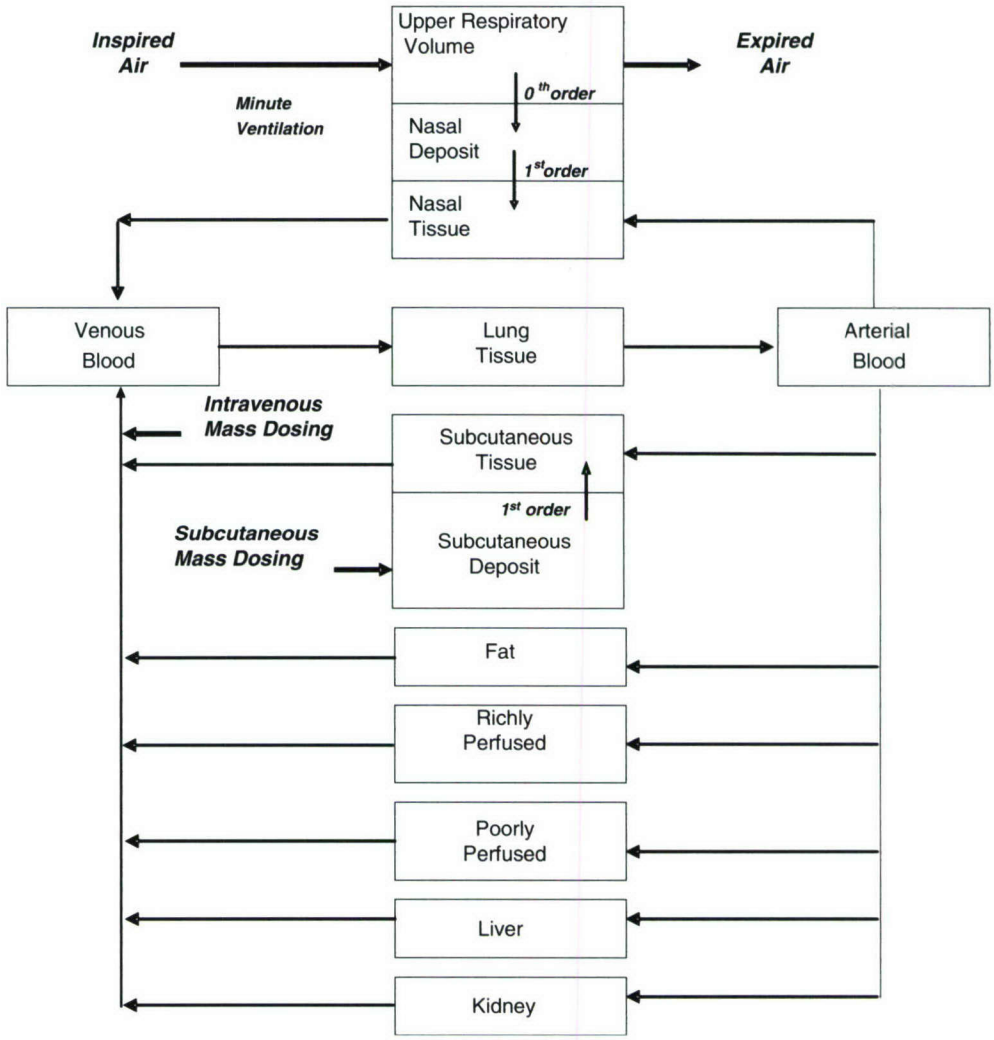

Fig. 1 Structure of the PB/PK model showing the blood flow between modeled compartments and the sites and mechanisms used for the modeled exposure routes

Biochemical parameters

Table 1 presents the initial enzyme concentrations, soman hydrolysis rates, and blood–tissue partition coefficients for the model compartments in each of the modeled species. Initial CaE levels in the compartments were taken from De Jong et al. (1993). A volume-weighted average of the concentrations for brain and diaphragm was used for the richly perfused compartment. The skeletal muscle CaE value was used for the poorly perfused compartment. Initial CaE in the subcutaneous deposit was set to zero since the compartment represents a sub-dermal fluid pocket. Initial CaE in the nasal tissue compartment was set to the skeletal muscle value since a smooth muscle value was unavailable. Initial AChE levels in the compartments were taken from Langenberg et al. (1997) for guinea pig and from Maxwell et al. (1988) for the rat. In the absence of measured values, marmoset values were set equal to the guinea pig values because of the close relationship of AChE distribution between nonhuman primates and guinea pigs (Silver 1974). The initial AChE in the richly perfused compartment was a volume-weighted average of the brain, heart and diaphragm values for guinea pig and rat. The skeletal muscle values were used for the poorly perfused compartment, nasal and subcutaneous compartments. Hydrolysis of soman was considered of significance in only the blood, kidney and liver compartments. The value for guinea pig plasma reported by Langenberg et al. (1997) was multiplied by the hematocrit and used for whole blood. Values for rat and marmoset plasma and for liver of the three species were taken from De Jong et al. (1998). Hydrolysis rate constants for guinea pig were taken from Langenberg et al. (1997) for the separate stereoisomers. Rate constants for kidney (DFPase modulated) hydrolytic activity in rats were reported by Maxwell et al. (1988). Since no data was available for marmoset kidney, a value of zero was used. In effect, this removes this process from the model for the marmoset kidney. Tissue–blood partition coefficients for the compartments were computed from values presented by Langenberg et al. (1997) for guinea pigs with the exception of a value for the fat compartment, which was adjusted to a value of 6.0 to fit the terminal half-life of the guinea pig and marmoset concentration profiles as was done in Langenberg's model.

Table 1 Enzyme initial concentrations, partition coefficients, and soman hydrolysis rates (min^{-1}) by species and model compartment

	Guinea pig (500 g)	Rat (250 g)	Marmoset (375 g)
Carboxylesterase (nM)			
Lung tissue	275[a]	6,870[a]	220[a]
Kidney	11,000[a]	12,100[a]	3.300[a]
Liver	65,900[a]	49,500[a]	13,700[a]
Poorly perfused	330[b]	470[b]	110[b]
Richly perfused	460[b]	210[b]	590[b]
Subcutaneous tissue	0[c]	0[c]	0[c]
Nasal tissue	330[d]	470[d]	110[d]
Fat	0[a]	0[a]	0[a]
Blood	440[a]	2,530[a]	3[a]
Acetylcholinesterase (nM)			
Lung tissue	4.50[e]	1.94[f]	4.50[g]
Kidney	4.44[e]	0.476[f]	4.44[g]
Liver	6.30[e]	0.891[f]	6.30[g]
Poorly perfused	1.60[e]	6.61[f]	1.60[g]
Richly perfused	49.10[e]	26.80[f]	49.10[g]
Subcutaneous tissue	1.60[h]	6.61[h]	1.60[h]
Nasal tissue	1.60[h]	6.61[h]	1.60[h]
Fat	0[d]	0[d]	0[d]
Blood	9.70[e]	9.70[e]	9.70[e]
C(+)P(−) Hydrolysis (min^{-1})			
Kidney	0.252[e]	1.310[f]	0.000[i]
Liver	0.600[j]	1.870[j]	0.667[j]
Blood	0.050[e]	0.125[i]	0.100[i]
C(−)P(−) Hydrolysis (min^{-1})			
Kidney	0.3[e]	1.31[f]	0.000[j]
Liver	0.1[j]	2.93[j]	1.267[j]
Blood	0.0[e]	0.267[j]	0.46[i]
Blood/tissue partition coefficient (used for all species)			
Lung tissue		0.55[e]	
Kidney		1.10[e]	
Liver		1.90[e]	
Poorly Perfused		0.75[e]	
Richly Perfused		0.49[e]	
Fat		6[k]	
Subcutaneous injection site		0.45[h]	
Nasal tissue deposition site		0.45[h]	

[a]Data from De Jong et al. (1993); richly and poorly perfused values are weighted averages of appropriate tissues
[b]Values calculated using a volume-weighted average of the appropriate tissues from De Jong et al. (1993)
[c]Value set to zero
[d]Value set to skeletal muscle number reported by De Jong et al. (1993)
[e]Data from Langenberg et al. (1997)
[f]Data from Maxwell et al. (1988)
[g]Values were set to the guinea pig values
[h]All injection site compartments were set to the muscle value
[i]No data available
[j]Data from De Jong et al. (1998)
[k]Fat compartment value was adjusted to fit data; acting as a nonreactive storage depot

The rate constants for soman interactions with carboxylesterase and acetylcholinesterase and the first-order soman adsorption rates used in the model are presented in Table 2. The bimolecular rate constants for the AChE and C(±)P(−)-soman were set to the human values presented in Ordentlich et al. (1999). This model uses human soman-AChE bimolecular rate constants for all compartments and for all species. Several bimolecular rate constants for the reaction of C(±)P(±)-soman (Maxwell et al. 1991) and C(+)P(−)-soman (De Jong et al. 1993; Benschop and De Jong 2001) with CaE have been reported. We used the blood C(+)P(−)-soman value from Benschop and De Jong (2001). The C(−)P(−)-soman rate constant was set to one-third of the C(+)P(−)-soman value based on previous observation of the relative reaction rates of C(+)P(−) and C(−)P(−) stereoisomers with CaE (Langenberg et al. 1997).

Physiological parameters

Table 3 presents the tissue volumes and flows for each compartment. To estimate the volume for the nasal tissue compartment we used surface area of 27.4 cm^2 for guinea pig nasal cavity (from Newton 2002) and estimated a depth 2 mm for the nasal mucosal layer and underlying tissue affected by local agent deposition. The resulting volume was 1% of the body volume. The flow for the compartment was estimated as 1% of the cardiac output using a volume-based weighting. The same methodology (98% adsorption in six adsorption half-lives) that was used by Maxwell et al. (1988) was used to estimate an absorption rate constant for the subcutaneous deposit based on RBC AChE inhibition data in guinea pigs during subcutaneous exposures (T.-M. Shih, unpublished data). The nasal absorption rate was estimated from correlation equations for compounds with similar log *P* values published in Fiserova-Begerova and Hughes (1983).

Sensitivity analysis

In a complex system, the observer can focus on an individual output and measure the change that results when only one input is changed. A normalized sensitivity (of an output to an input) is defined as the percentage change in the output divided by the percentage change in the input that caused the output to change. The computed value describes (as the name implies) how sensitive the output is to that input. Sensitivity can be computed at each time point during a simulation to construct a time-series indicating how the output is affected by changes in the input at each time during the simulation. In the sensitivity analysis we have performed, we have focused on the arterial C(−)P(−)-soman concentration as the output, but have computed sensitivity curves for each parameter in the model for each dosing condition for guinea pigs. The sensitivity curves describe the influence of each model parameter on the arterial soman level at any time during the model simulations. The sensitivities were calculated for small (approximately 4%) perturbations in each parameter and can be compared to each other to determine which model parameters are most important at different times during a simulation.

Table 2 Rate constants used in the model

		C(+)P(−)-soman	C(−)P(−)-soman
Bimolecular	AChE[a]	1.5×10^8	8.0×10^7
Bimolecular	CaE[b]	3.0×10^7	1.0×10^6
Absorption	Subcutaneous[c]	1.9	1.9
Absorption	Nasal	1.0	1.0

Units are M^{-1} min^{-1} for bimolecular constants and min^{-1} for absorption constants

[a]AChE–soman bimolecular rate is human value reported by Ordentlich et al. (1999)

[b]Values from Benschop and De Jong (2001)

[c]From Maxwell et al. (1988) and T.-M. Shih (unpublished data)

Results

Simulations

The model was used to simulate intravenous, subcutaneous, and inhalation exposures of guinea pigs, rats, and marmosets to high ($6 \times LD_{50}$), medium ($2–3 \times LD_{50}$), and low ($0.4–1.0 \times LD_{50}$ or LCt_{50}) doses of soman. The LD_{50} and LCt_{50} values used are shown in Table 4. Model validation was done by comparing measured (Benschop and De Jong 2001; Due et al. 1994) arterial concentrations of C(+)P(−) and C(−)P(−)-soman after various exposures against simulated arterial concentration profiles. Simulation results are presented in Figs. 2, 3, 4, and 5. The lighter curve in each plot corresponds to the simulated C(+)P(−)-soman concentration; the darker curve, to the C(−)P(−)-soman concentration. The plotted data points indicate observed concentrations of C(+)P(−)-soman (open squares) and C(−)P(−)-soman (open circles). Error bars (when available) indicate the 95% confidence limits of the observations. Insets in each graph provide more detail for early time points.

Table 3 Physiological parameters computed allometrically by species and model compartment

	Guinea pig	Rat	Marmoset
Minute ventilation (ml min^{-1}) 213	125	164	164
Cardiac output (ml min^{-1})	147	84	112
Flow (% of C.O.)			
Kidney	11.4	11.4	11.4
Liver	18.0	18.7	18.4
Poorly Perfused	26.0	23.7	24.9
Richly Perfused	42.8	44.7	43.7
Fat	0.7	0.6	0.7
Subcutaneous tissue	0.01	0.01	0.01
Nasal tissue	1.0[a]	1.0[b]	1.0[b]
Volume (% of B.W.)			
Lung tissue	0.5	0.5	0.5
Kidney	0.9	1.0	1.0
Liver	3.8	4.1	4.0
Poorly perfused	81.3	81.9	81.6
Richly perfused	5.4	5.2	5.3
Fat	1.4	1.0	1.2
Subcutaneous tissue	0.1	0.1	0.1
Nasal tissue	1.0[a]	1.0[b]	1.0[b]
Arterial blood	1.6	1.5	1.6
Venous blood	3.8	3.6	3.7

[a]Nasal tissue compartment flow was set to tissue–volume weighted average of the cardiac output. Nasal tissue volume from nasal cavity surface area (Newton 2002) and a mucosa/tissue depth estimate of 2 mm

[b]Rat and marmoset assigned the same flow and volume percentages as the guinea pig

Table 4 Racemic soman LD_{50} and LCt_{50} values by species and exposure route

Guinea pig	Intravenous	27.5 μg kg^{-1}
	Subcutaneous	24.7 μg kg^{-1}
	8 min inhalation	48.0 mg min m^{-3}
Rat	Intravenous	82.5 μg kg^{-1}
Marmoset	Intravenous	10.0 μg kg^{-1}

Figure 2 presents the arterial soman profiles in guinea pigs for simulations of high-, medium- and low-dose intravenous bolus injections (panels a, b, c); a high-dose subcutaneous injection (panel d); and an 8-min low-dose intravenous infusion (panel e). The simulations for these exposures lie within the measured confidence limits except for the 2- and 4-min C(+)P(−)-soman measurements taken during the 8-min intravenous infusion exposure. No confidence limits are available for the subcutaneous exposure. Figure 3 presents arterial soman profiles for simulations of high-, medium-, and low-dose intravenous bolus injections of soman in rats (panels a, b, c), while Fig. 4 presents the arterial concentrations for high- and medium-dose intravenous exposures in marmosets (panels a, b). No low-dose data is available for marmoset. The simulations for these exposures generally lie within the 95% confidence limits. Where the model deviates from the measured data, the simulated values still lie within the 99% confidence limits (not shown) of the measured data. Inhalation exposure simulations in guinea pigs are presented in Fig. 5 and include profiles for an 8-min $0.4 \times LCt_{50}$ exposure (panel a), 4- and 8-min $0.8 \times LCt_{50}$ exposures (panels b, c), and a 300-min $0.1 \times LCt_{50}$ exposure (panel d). The simulated values for these exposures lie within the 95% confidence limits for the short-term exposures except for the 2- and 4-min C(+)P(−)-soman measurements. The simulated values for the 300-min inhalation exposure (panel d) lie within the 95% confidence limits for data measured during the exposure, but fall much too quickly after the exposure ends.

Regression analysis

To quantify the model fit to observed data points, the points on the simulated arterial soman profiles at times when observed data was available were plotted against the observed data to form "predicted versus observed" graphs. Logs (base 10) of the values were used to weight the data. For a perfect model fit, all of the graphed points would fall on the line through the origin with unity slope. A linear regression (with an intercept of zero) was performed for each soman stereoisomer and

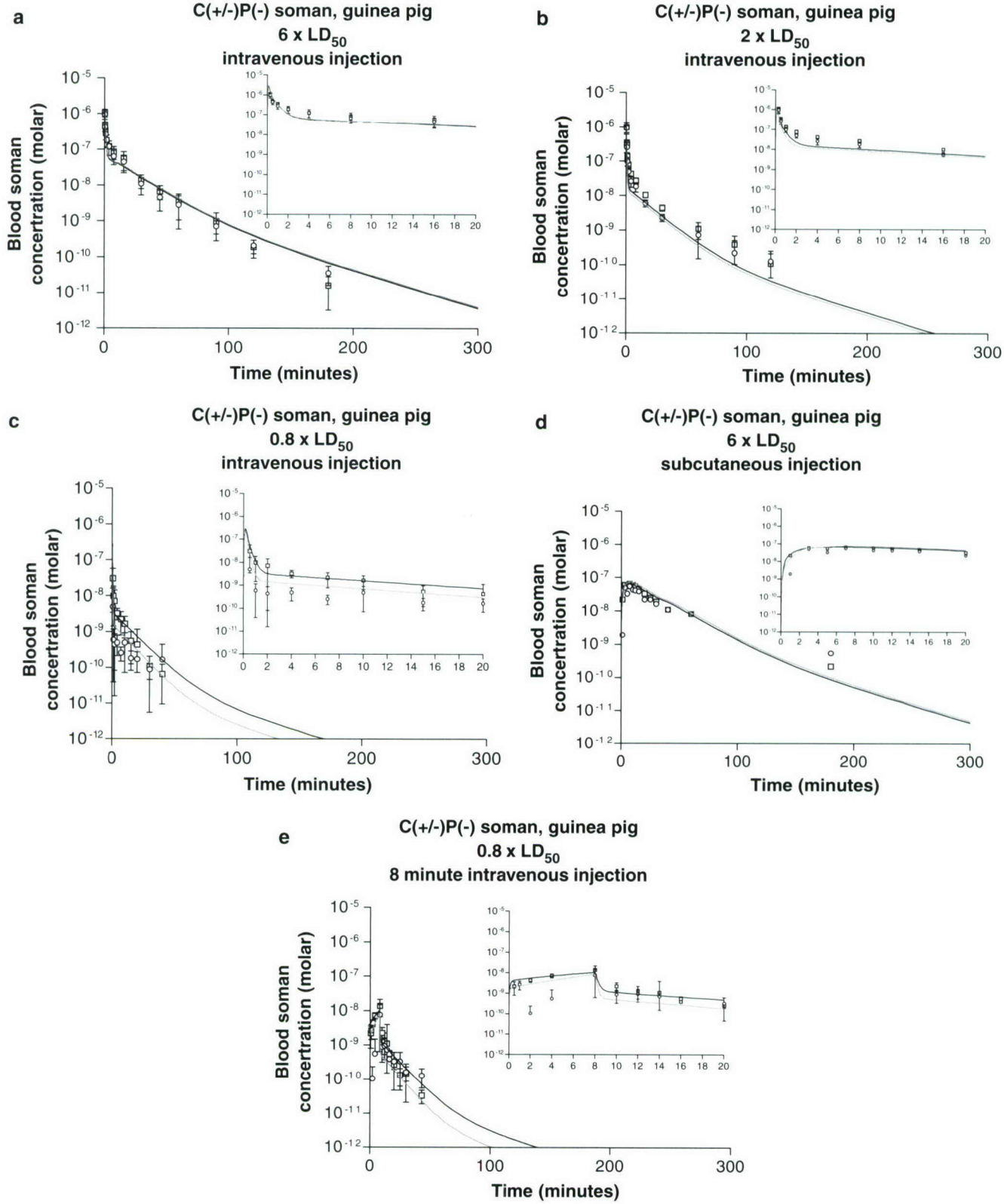

Fig. 2 Simulated arterial C(−)P(−)-soman (*dark curve*) and C(+)P(−)-soman (*light curve*) concentrations in guinea pigs after several dose levels and exposure routes. *Insets* show detail at early time points. Plotted points (Benschop and De Jong 2001) show measured arterial C(−)P(−)-soman (*squares*) and C(+)P(−)-soman (*circles*) concentrations with 95% confidence intervals

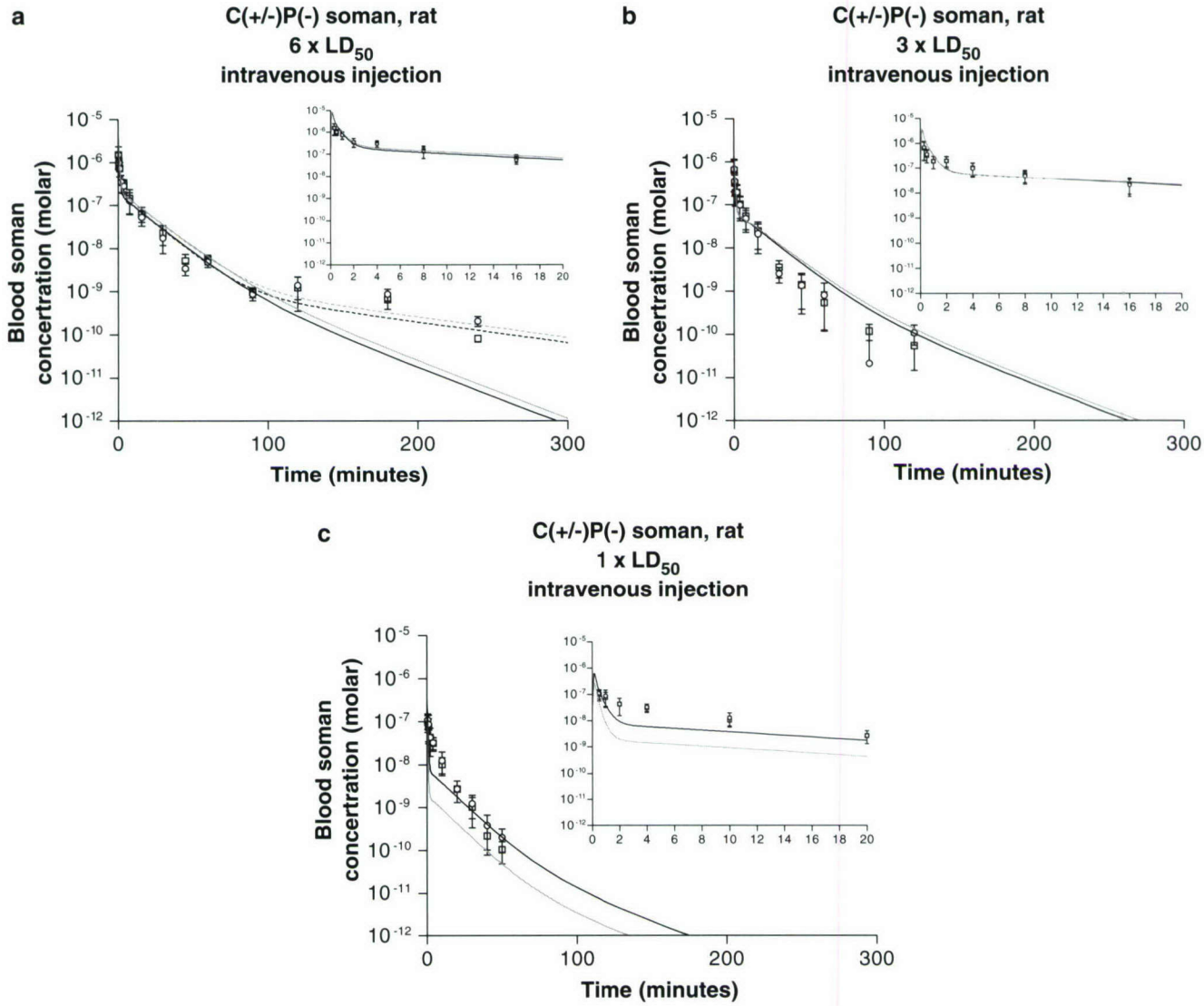

Fig. 3 Simulated arterial C(−)P(−)-soman (*dark curve*) and C(+)P(−)-soman (*light curve*) concentrations in rat for several intravenous exposure levels. *Insets* show detail at early time points. Plotted points (Benschop and De Jong 2001) show measured concentration of arterial C(−)P(−)-soman (*squares*) and C(+)P(−)-soman (*circles*) concentrations with 95% confidence intervals. *Dashed curves* in panel **a** indicate simulated concentrations with an increased fat partition coefficient (to compensate for a possible second soman storage depot)

each model simulation. The correlation coefficient (r) describing the scatter of points about this line is given in Table 5 for each soman stereoisomer and each model simulation. The C(−)P(−)-soman correlation coefficients were higher than the C(+)P(−)-soman coefficients in 12 of the 14 exposures. Intravenous simulations for $1.0 \times LD_{50}$ or higher doses match the measured data with a correlation coefficient greater than 0.912. The lowest intravenous dose tested ($0.8 \times LD_{50}$) had the poorest fit of all intravenous data sets with a correlation coefficient of 0.863 for the C(+)P(−)-soman stereoisomer. The subcutaneous simulation matched the measured data with correlation coefficients greater than 0.893. For intravenous infusion, the C(+)P(−)-soman simulation (0.665) did not fit as well as the C(−)P(−)-soman fit (0.913) due to the points measured at 2 and 4 min. With these two points omitted, the C(+)P(−)-soman fit improves to 0.953, but the C(−)P(−)-soman fit falls to 0.851. The inhalation simulations (4 data sets) did not fit the measured data as well as the other exposures with correlation coefficients in the range 0.298–0.913. The short-term inhalation exposures (8 min or less) showed correlation coefficients (0.664–0.913) that were much better than coefficients for the long term, lower dose, 300-min exposure (0.298, 0.417).

Sensitivity analysis

The sensitivities of the simulated arterial C(−)P(−)-soman concentration to changes in the model parameters are presented in Fig. 6a–f. The sensitivity analyses were

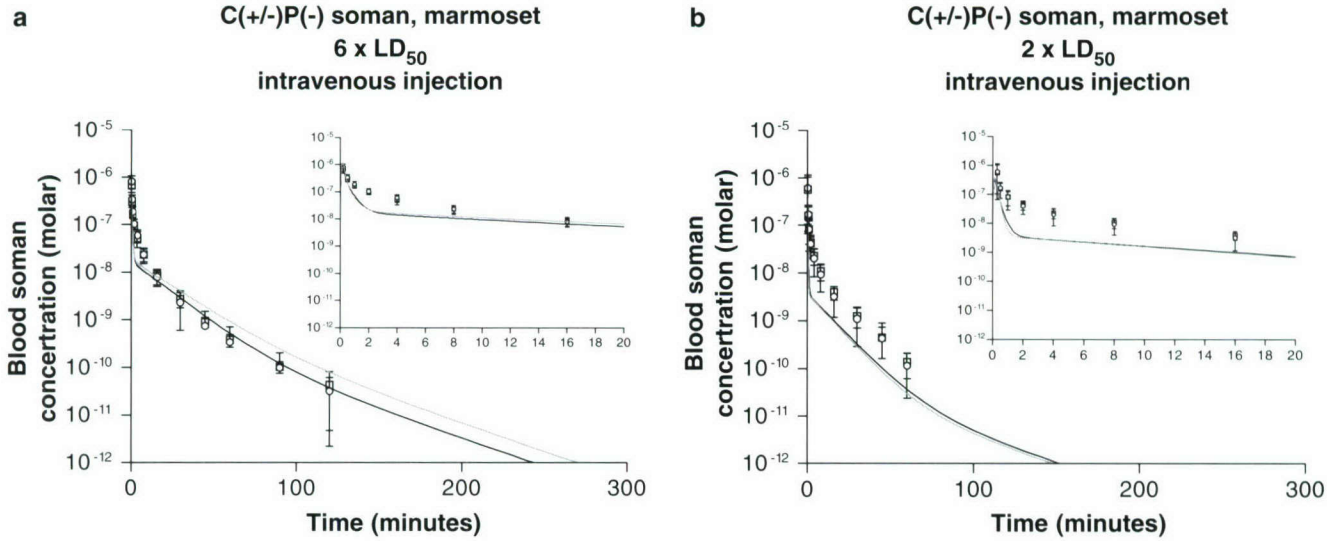

Fig. 4 Simulated arterial C(−)P(−)-soman (*dark curve*) and C(+)P(−)-soman (*light curve*) concentrations in marmoset for high- and medium-dose intravenous exposures. *Insets* show detail at early time points. Plotted points (Benschop and De Jong 2001) show measured arterial C(−)P(−)-soman (*squares*) and C(+)P(−)-soman (*circles*) concentrations with 95% confidence intervals

limited to one stereoisomer of soman and were carried out for all guinea pig simulations to allow comparison of sensitivities between intravenous, subcutaneous, and inhalation exposures. These graphs indicate the relative importance of the parameters during the simulations. Note that the time axis is plotted on a logarithmic scale. Figure 6a shows the sensitivities to perturbations in the partition coefficients for most compartments. Figure 6b breaks out the sensitivities to partition coefficients for the subcutaneous and nasal tissue compartments. Figure 6c presents the sensitivities of arterial soman concentration to the absorption rate constants used for the injection site compartments for the corresponding exposures. The sensitivities to absorption rates were uniformly zero for intravenous exposures and are not presented. Figure 6d, e depicts the sensitivity of the arterial soman concentration to each of the bimolecular rate constants in the model for intravenous exposures (Fig. 6d) and all other exposures (Fig. 6e). Note that the rate constants for binding with both the C(+)P(−)-soman and the C(−)P(−)-soman stereoisomers are included. Figure 6f shows the sensitivity of the arterial C(−)P(−)-soman concentration to the hydrolysis rates in the three hydrolyzing compartments (liver, kidney and plasma).

The sensitivities generally remain less than five for all parameters. A sensitivity discontinuity occurs around 10 min (Fig. 6b), which is due to computational artifacts in the sensitivity algorithm. A high value for the sensitivity of the arterial soman concentration to the partition coefficient for a compartment is an indication that a net transport is occurring between the compartment and the blood, since the transport terms in the underlying equations are the only places where the partition coefficients appear in the model. A positive sensitivity indicates transport into the blood. In Fig. 6a, it is apparent that the partition coefficient in the fat compartment has a progressively greater influence as time increases past 100 min. This indicates that the rate at which soman is returned from the non-reactive fat depot has a major influence on the arterial concentration late in the simulations. In the 10–100 min range, the arterial concentration is most sensitive to the partition coefficient of the poorly perfused compartment with a peak around 2.5 at 70 min. In that compartment, there is a trend for the partition coefficient sensitivities to be negative at earlier times (indicative of net soman flux into the compartment) and to become positive at later times. By roughly 10 min, the net transport into the poorly perfused compartment has reversed. By 120 min, more soman is leaving the fat compartment than is leaving the poorly perfused compartment, but both are returning soman to the blood. The partition coefficient for the lung compartment exhibits the greatest sensitivity very early (less than 1 min) for the subcutaneous exposure. The fact that the sensitivity is negative indicates that net soman transport is into the lung during this period. Figure 6b shows that the partition coefficient assigned to an exposure site compartment has an effect only when the exposure is via that site. Similarly, Fig. 6c indicates that the absorption rate for an exposure compartment is important only for exposures through the compartment.

The sensitivities of the arterial soman concentration to the bimolecular reaction rate constants are shown in Fig. 6d (intravenous bolus exposures) and Fig. 6e (all other exposures) and indicate that, of the four binding rate constants, the reaction of CaE with C(−)P(−)-soman has the greatest impact. This effect appears only during the low- dose exposure because CaE is depleted quickly during the high- and medium-dose exposures. Increases in the rate constant for CaE binding with C(+)P(−)-soman actually increases arterial C(−)P(−)-soman because relatively more of the CaE is bound to C(+)(Pc)-soman as that rate constant increases, leaving

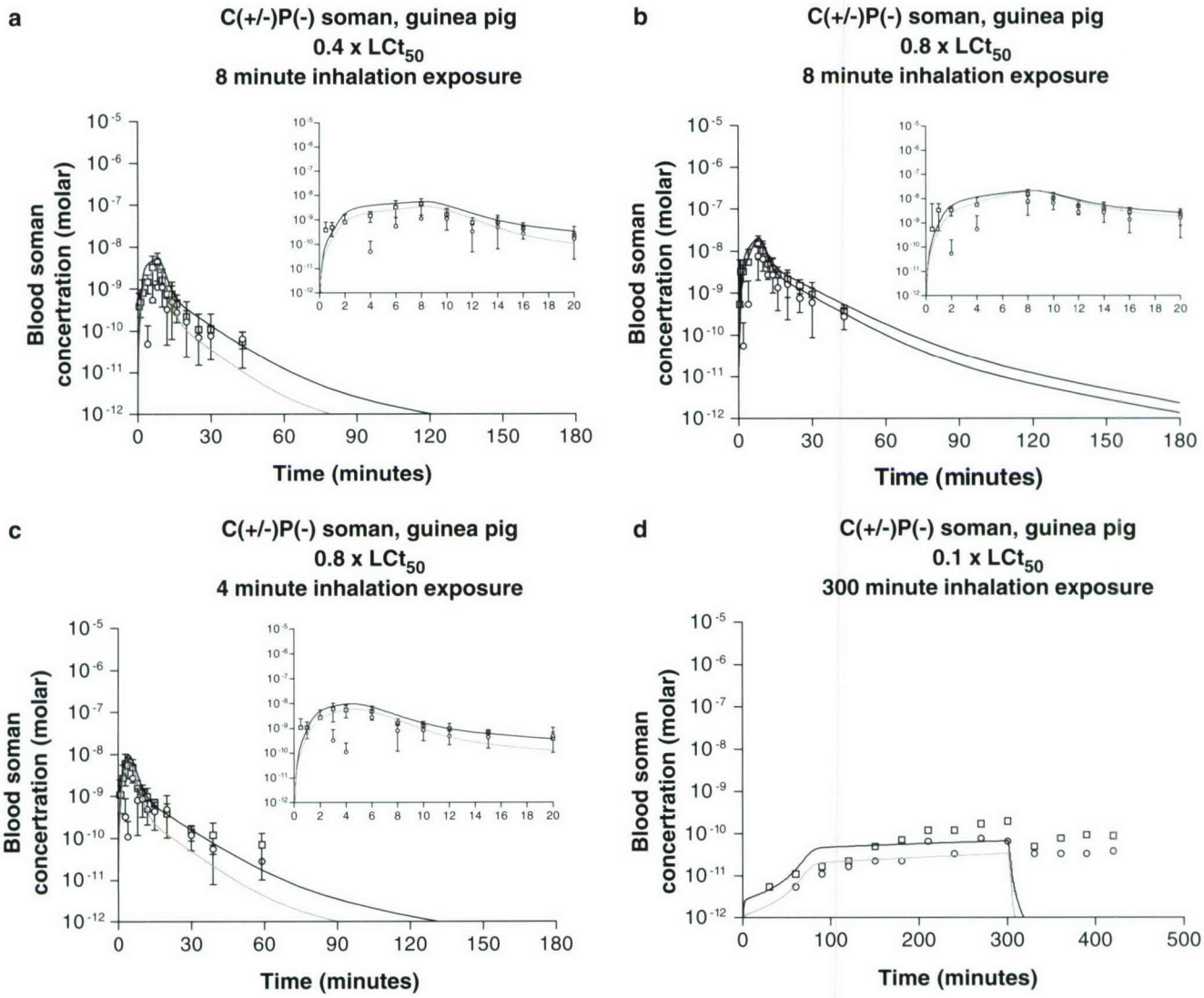

Fig. 5 Simulated arterial C(−)P(−)-soman (*dark curve*) and C(+)P(−)-soman (*light curve*) concentrations in guinea pigs for several inhalation exposures. *Insets* show detail at early time points. Plotted points (Benschop and De Jong 2001) show measured arterial C(−)P(−)-soman (*squares*) and C(+)P(−)-soman (*circles*) concentrations with 95% confidence intervals

less available to bind C(−)P(−)-soman. Sensitivity of the soman concentration to the AChE binding rate is small because the AChE levels are roughly three orders of magnitude lower than the soman levels. Lastly, it should be noted from Fig. 6f that the sensitivities to the hydrolysis rates are small at all times when the dose is low. When the administered dose is high, hydrolysis becomes important late in the profile. For high doses, the CaE becomes diminished after roughly 80–100 min, and hydrolysis/elimination takes over as the major detoxification mechanism.

Discussion

The simulated arterial C(+)P(−)-soman and C(−)P(−)-soman concentrations generally fall within the 95% confidence limits of the measured concentrations for subcutaneous and intravenous bolus exposures in guinea pigs, rats, and marmosets. Almost all of the simulated values falling outside of the 95% limits still lie within the 99% confidence limits. For the 8-min intravenous infusion exposure, the early time points for the C(+)P(−)-soman predictions are too high. During this infusion period, the difference between the measured soman stereoisomers is the largest seen for any of the intravenous exposures. A similar difference between the C(+)P(−)-soman stereoisomer and the C(−)P(−)-soman stereoisomer was also measured in the early time points of the 8-min inhalation exposures. The simulated soman values fall within 95% confidence limits of the measured values for these inhalation exposures with the exception of the early C(+)P(−)-soman measurements at 2 and 4 min. It seems clear that some process not included in our model is differentially reducing the concentration of the C(+)P(−) stereoisomer during the initial phase of both

Table 5 Coefficients of correlation (r) for the line "Log (simulated data) = Log(observed data)" for both P(−)-soman stereoisomers under different modeling simulations

Simulation (by route, dose, species)	C(+)P(−)-soman	C(−)P(−)-soman
Intravenous		
$6.0 \times LD_{50}$ in rat	0.935	0.956
Without points > 180 min	0.964	0.968
All points, fat part. coeff. (6 → 17)	0.976	0.982
$3.0 \times LD_{50}$ in rat	0.968	0.974
$1.0 \times LD_{50}$ in rat	0.913	0.912
$6.0 \times LD_{50}$ in marmoset	0.963	0.979
$2.0 \times LD_{50}$ in marmoset	0.975	0.981
$6.0 \times LD_{50}$ in guinea pig	0.987	0.982
$2.0 \times LD_{50}$ in guinea pig	0.986	0.990
$0.8 \times LD_{50}$ in guinea pig	0.863	0.944
Without 40 min point	0.964	0.932
Subcutaneous		
$6.0 \times LD_{50}$ guinea pig	0.893	0.982
8 min intravenous infusion		
$0.8 \times LD_{50}$ guinea pig	0.665	0.913
Without 2 and 4 min points	0.953	0.851
Inhalation exposure in guinea pig		
$0.8 \times LCt_{50}$ (8 min exposure)	0.706	0.664
$0.8 \times LCt_{50}$ (4 min exposure)	0.669	0.913
$0.4 \times LCt_{50}$ (8 min exposure)	0.755	0.901
$0.1 \times LCt_{50}$ (300 min exposure)	0.298	0.417

the intravenous infusion and inhalation exposures. In fact, during the 300-min inhalation exposure (Benschop and De Jong 2001), the C(+)P(−)-soman stereoisomer was not detected in the arterial blood until 60 min into the exposure. The simulated soman concentrations for this long-term exposure fall within the 95% confidence limits for the measured data during the exposure period, but fall much too quickly after the exposure ends. This suggests that the model overestimates the elimination of soman at this low dose. It should be noted that for this dataset the errors in the observed values, when expressed as a percentage of the mean, are the largest of any of the datasets. An evaluation of the model's performance based on a review of the simulation curves and the confidence intervals for the measured data suggests that the model performs better for the C(−)P(−)-soman stereoisomer than for the C(+)P(−)-soman stereoisomer, better for high doses than for low doses, and better for intravenous and subcutaneous exposures than for inhalation exposures.

The regression analysis of predicted versus measured concentration values allowed us to quantify the model's performance for the 28 available datasets. The conclusions reached by regression analysis agreed with the conclusions drawn from our comparison of the simulations with the confidence limits of the observed data. The simulations for high ($6 \times LD_{50}$), medium ($2–3 \times LD_{50}$), and low ($0.8–1.0 \times LD_{50}$) doses match the observed data well for intravenous exposures (Figs. 2a–c, 3, 4) across species. The average correlation coefficients for those simulations are 0.954 ± 0.044 for the C(+)P(−) stereoisomer and 0.968 ± 0.026 for the C(−)P(−) stereoisomer. The lowest correlation coefficient for intravenous exposures was 0.863 for the low-dose guinea pig simulation (Fig. 2c). This value was improved to 0.936 by the removal of one observed data point at 40 min. The simulations of medium level challenges in both rats and marmosets (Figs. 3, 4) tend to predict values greater than the observed data points, while the low-dose simulations tend to predict values lower than the observed data.

For the high-dose rat simulation (Fig. 3a), the model predicts concentrations that are much lower than the measured concentrations at the time points above 100 min. It can be seen from the sensitivity curves presented in Fig. 6a that the arterial soman concentration is most sensitive to the partition coefficient in the fat compartment after approximately 100 min post-exposure. Subsequently, an adjustment of the partition coefficient of the fat compartment in rats (from 6 to 17) was found to fit these points (shown as dotted lines in Figure 3a). While having little effect on the early time points, this change alters the simulated response at later times. It is unlikely that the partition coefficient for fat would vary by a factor of three between the species. However, the fat compartment in this model functions as a reaction-free soman depot, which suggests that the model should include a second such depot, possibly a bladder compartment. There is evidence (Benschop and De Jong 2001) that soman excreted into the bladder is reabsorbed into the body and that the degradation rate in the urine is very low. Under these conditions, the bladder forms a nonreactive storage depot functionally similar to the fat compartment in our model. The adjustment of the fat partition coefficient in the rat is thought to be compensating for the absence of the second reaction free compartment. It is likely that this effect is seen in rats, but not in guinea pigs or marmosets because the absolute dose administered in rat is much higher than in the other species.

The high-dose guinea pig subcutaneous exposure simulation (Fig. 2d) matches the C(+)P(−)-soman observations well ($r = 0.893$) and the C(+)P(−) observations quite well ($r = 0.982$). The fits for the C(−)P(−) stereoisomer are generally better than for the C(+)P(−) stereoisomer across all simulations. A difference between the observed stereoisomer is prominent during the 8-min intravenous infusion dataset (Fig. 2e). In the simulation for that exposure, the C(+)P(−) stereoisomer ($r = 0.665$) does not fit as well as C(−)P(−) stereoisomer ($r = 0.913$) because the model overestimates the values for the 2-and 4-min C(+)P(−) data points. Without those points, the correlation coefficient rises to 0.953. The difference between the predictions for soman stereoisomers is most pronounced in the low-dose simulations. In the model, this occurs because the stereoisomers have different rates of combination with CaE, which exerts its greatest influence at the low doses (see Fig. 6d).

The inhalation exposure results for the short-term exposures (i.e., 4 and 8 min) for both stereoisomers are shown in Fig. 5a–c. The means and standard errors of

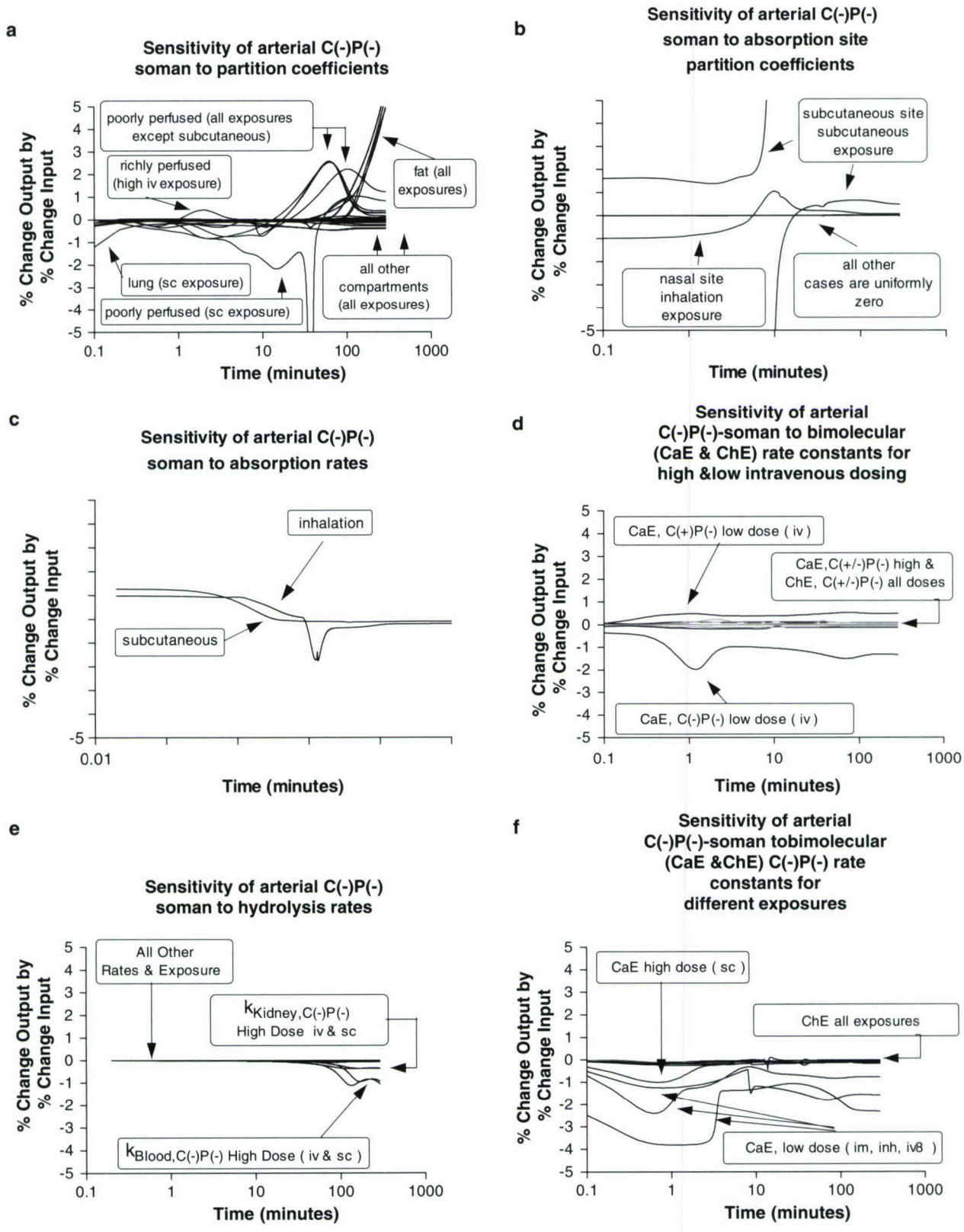

Fig. 6 Sensitivity of arterial C(−)P(−)-soman simulation to model parameters for guinea pig exposures. At each time point, the curves indicate the percentage that the arterial C(−)P(−)-soman concentration would change in response to a 1% increase in the model parameter associated with the curve. The *curves* show the relative influence that each model parameter exerts on the C(−)P(−)-soman concentration as the simulation progresses. Sensitivity curves may be numerically compared

the correlation coefficients for those simulations are 0.710 ± 0.043 for the C(+)P(−) stereoisomer and 0.827 ± 0.142 for the C(−)P(−) stereoisomer, which is considered an adequate fit, but not as good as for the intravenous exposures. There is generally more scatter in the inhalation data set than in the other data sets, which is also reflected in the lower correlation coefficients that are seen with the inhalation data. It can be seen from Fig. 5d that the model simulates the overall pattern of the observed data points except for the post-exposure points at times greater than 300 min in the 300-min $0.1 \times LCt_{50}$ challenge. The correlation coefficients for this simulation are only 0.298 and 0.417, which are considered poor fits. The simulated responses fall off much too rapidly after the exposure ends at 300 min. Clearly, the reasons for this discrepancy must be explored in future work. Overall, the differences between the observed C(+)P(−)-soman and C(−)P(−)-soman stereoisomer concentrations are most evident during the exposure phases of the inhalation/infusion simulations and during the first minutes following subcutaneous exposure (while the bolus is being absorbed into the venous blood). During these exposure periods, the model predictions generally do not match the observed magnitude of the differences between the stereoisomers, but do show differences of lesser magnitudes.

Inaccuracies in the initial CaE values would be expected to have exaggerated effects for challenges below or near the critical $1 \times LD_{50}$ level. The high dose challenge simulations match measured data better than low-dose simulations. The argument can be made that the amount of soman that can be bound by CaE is the major determinant of the LD_{50}, so challenges above one LD_{50} result in depletion of any soman-accessible CaE. The fact that the high- and medium-dose exposure levels can be modeled adequately indicates that the model uses suitable values for the soman elimination rate constants (encompassing both excretion and hydrolysis), since only those processes would be active after the initial phase of the higher exposures.

Conclusions

We can form conclusions about model performance based upon the square of the correlation coefficients given in Table 5 that describe how well the predicted values match the measured values for each exposure. A correlation coefficient of 0.85 indicates that the model explains 72% of the variation in the measured data. Using 70% as our criterion, we can conclude that the model adequately predicts arterial C(±)P(−)-soman concentrations for short-term exposures to racemic soman by the intravenous, subcutaneous and inhalation routes in guinea pigs, rats, and marmosets. In its present form, the model does not adequately predict the long-term (300-min) inhalation exposure data, particularly in the post-exposure period. The current model performs better at exposure doses above $1 \times LD_{50}$ than it does at doses below $1 \times LD_{50}$. An important feature of this model is the inclusion of a reactive nasal tissue compartment, which allowed the measured inhalation data to be predicted. A similar reactive injection site tissue compartment, from which the nerve agent is absorbed into the remainder of the body, proved to be suitable for modeling the available subcutaneous data. A similar technique will be employed to model percutaneous exposures when data to validate them becomes available. Since the species-dependant parameters to extrapolate between species can be determined from in vitro measurements on tissue samples, it should be possible to predict toxicokinetics for soman in humans. With an underlying model in place, our modeling effort can now be shifted towards studies of other nerve agents and the toxicokinetic effects of scavenger enzymes injected into the body for protection against nerve agent challenge (Lenz et al. 2001).

Acknowledgments This work was supported by the US Army Medical Research Institute of Chemical Defense and partly through the Army Research Office contract DAA019-02-0-0001 (DO 0573), administered by Battelle. No animals were used in this modeling effort. All animal observations were obtained from previously published sources.

References

Ainsworth M, Shephard RJ (1961) The intrabronchial distribution of soluble vapours at selected rates of gas flow. In: Davies CN (ed) Inhaled particles and vapours. Pergamon Press, pp 233–247

Benschop HP, De Jong LPA (2001) Toxicokinetics of nerve agents. In: Somani SM, Romano JA (eds) Chemical warfare agents: toxicity at low levels. CRC Press, Boca Raton, pp 25–81

De Jong LPA, Van Dijk C, Berhitoe D, Benschop HP (1993) Hydrolysis and binding of a toxic stereoisomer of soman in plasma and tissue homogenates from rat, guinea pig, and marmoset, and in human plasma. Biochem Pharmacol 46(8):1413–1419

De Jong LPA, Van Dijk C, Benschop HP (1998) Hydrolysis of the four stereoisomers of soman catalyzed by liver homogenate and plasma from rat, guinea pig and marmoset, and by human plasma. Biochem Pharmacol 37(15):2939–2948

Due AH, Trap HC, Langenberg JP, Benschop HP (1994) Toxicokinetics of soman stereoisomers after subcutaneous administration to atropinized guinea pigs. Arch Toxicol 68:60–63

Fiserova-Bergerova V, Hughes HC (1983) Species differences on bioavailability of inhaled vapors and gases. In: Fiserova-Bergerova V (ed) Modeling of inhalation exposure to vapors: uptake, distribution, and elimination. vol 2, CRC Press, Boca Raton, pp 97–106

Gerlowski LE, Jain RK (1983) Physiologically based modeling: principles and applications. J Pharm Sci 72:1103–1127

Gibaldi M, Perrier D (1982) Pharmacokinetics. 2nd edn. Marcel Dekker, New York, pp 364–369

Langenberg JP, Van Dijk C, Sweeney RE, Maxwell DM, De Jong LPA, Benschop HP (1997) Development of a physiologically based model for the toxicokinetics of C(±)P(±)-soman in the atropinized guinea pig. Arch Toxicol 71:320–331

Lenz DE, Broomfield CA, Maxwell DM, Cerasoli DM, (2001) Nerve agent bioscavengers: protection against high- and low-dose organophosphorus exposure. In: Somani SM, Romano JA (eds) Chemical warfare agents: toxicity at low levels. CRC Press, Boca Raton, pp 25–81

Maxwell DM, Wolfe AD, Ashani Y, Doctor BP (1991) Cholinesterase and carboxylesterase as scavengers of organophosphorus agents. In: Massoulie J, Bacou F, Barnard E, Chatonnet A, Doctor BP, Quinn D (eds) Cholinesterase: structure, function, mechanism, genetics, and cell biology. American Chemical Society, Washington, pp 206–209

Maxwell DM, Vlahacos CP, Lenz DE (1988) A pharmacodynamic model for soman in the rat. Toxicol Lett 43:175–188

Newton PE (2002) Fundamental inhalation toxicology. In: Derelanko MJ, Hollinger MA (eds) Handbook of toxicology. CRC Press, Boca Raton, pp 267–334

Ordentlich A, Barak D, Kronman C, Benschop HP, De Jong LPA, Ariel N, Barak R, Segall Y, Velan B, Schafferman A (1999) Exploring the active center of human acetylcholinesterase with stereoisomers of an organophosphorus inhibitor with two chiral centers. Biochemistry 38:3355–3366

Silver A (1974) The biology of cholinesterases, Frontiers of biology. vol. 36, Elsevier, New York, pp 177–302

Arch Toxicol (2006) 80: 732–738
DOI 10.1007/s00204-006-0100-6

TOXICOKINETICS AND METABOLISM

H. Kamimura

Genetic polymorphism of cytochrome P450s in beagles: possible influence of CYP1A2 deficiency on toxicological evaluations

Received: 15 March 2006 / Accepted: 22 March 2006 / Published online: 26 April 2006

Abstract A number of human cytochrome P450 (CYP) isozymes have been shown to be genetically polymorphic, and extensive pharmaceutical studies have been conducted to characterize the clinical relevance of the polymorphism. Although the beagle is extensively used in the safety assessment studies of new drug candidates and agricultural chemicals, only a limited number of studies have been reported on the significance of the CYP isozyme polymorphism in dogs. Recently, a single nucleotide polymorphism that results in a deficiency of canine CYP1A2 was discovered. This deficiency was shown to significantly alter the pharmacokinetic behavior of two drugs, and can be associated with a large inter-individual difference in the kinetic behavior of a third. In this article, the five genetically polymorphic canine CYP isozymes that have been reported so far are reviewed, and the altered pharmacokinetics of the drugs concerned are described. Although little information on toxicological relevance has been reported, it is possible that the modified pharmacokinetics may also cause altered toxic responses as well. This phenomenon may occur only with the types of chemicals that are eliminated mainly through polymorphic-enzyme mediated metabolism. However, it is recommended that genetically pure beagles are used for the toxicity studies and safety assessment of new chemical entities in order to reduce the potential inter-individual differences.

Keywords Beagle dogs · Genetic polymorphism · Cytochrome P450 · SNPs · Toxicokinetics

H. Kamimura
Drug Metabolism Research Laboratories,
Astellas Pharma Inc., Azusawa 1-1-8, Itabashi-ku,
Tokyo 174-8511, Japan
E-mail: hidetaka.kamimura@jp.astellas.com
Tel.: +81-3-59162160
Fax: +81-3-39606220

Introduction

It is known that some collies (30–40%) are extremely susceptible to the neurotoxicity induced by ivermectin, a semi-synthetic antiparasitic. This phenomenon is due to a deletion mutation of the MDR1 gene, resulting in the lack of mature P-glycoprotein, which in turn causes ivermectin not to be extruded from the brain tissue into the blood (Mealey et al. 2001). Meanwhile, single nucleotide polymorphisms (SNP) in the thiopurine S-methyltransferase of domestic dogs are associated with the reduced activity of this enzyme, and, consequently, serious thiopurine-related toxicity (Salavaggione et al. 2002). These are typical, but rare, examples reported for dogs that demonstrate how toxicological responses to given drugs are enhanced by genetic polymorphism.

Cytochrome P450 (CYP) is categorized as belonging to a superfamily of physiologically important enzymes for the metabolism of endogenous and exogenous compounds (Danielson 2002; Nebert and Russell 2002). Many of the 63 human CYP genes are polymorphic (Ingelman-Sundberg et al. 1999; Nelson 1999; Orphanides and Kimber 2003), and the clinical relevance of the polymorphism has extensively been studied. This is particularly true for pharmaceutically important isoenzymes such as CYP2A6 (Nunoya et al. 1999), CYP2C9 (Sullivan-Klose et al. 1996), CYP2C19 (Furuta et al. 1999), and CYP2D6 (Meyer et al. 1986; Kagimoto et al. 1990). Because of their appropriate body weight and ease of handling (particularly during blood sampling), beagle dogs are used extensively for the drug discovery and safety assessment of chemical entities. To date, nine canine CYP isozymes have been identified through cloning and sequencing techniques, five of which have been reported as genetically polymorphic. Until recently, little has been discovered about the polymorphism directly associated with altered xenobiotic metabolism. In this article, a series of studies on the genetic polymorphism of canine CYPs is reviewed with the focus on the recent discovery of